Crystal and magnetic structure of Mn_3IrSi

T. Eriksson,[1] R. Lizárraga,[2] S. Felton,[3] L. Bergqvist,[2] Y. Andersson,[1] P. Nordblad,[3] and O. Eriksson[2]
[1]*Department of Materials Chemistry, Uppsala University, Box 538, 751 21 Uppsala, Sweden*
[2]*Department of Physics, Uppsala University, Box 530, 751 21 Uppsala, Sweden*
[3]*Department of Materials Science, Uppsala University, Box 534, 751 21 Uppsala, Sweden*
(Received 1 September 2003; published 24 February 2004)

A new ternary Ir-Mn-Si phase with stoichiometry Mn_3IrSi has been synthesized and found to crystallize in the cubic $AlAu_4$-type structure, space group $P2_13$ with $Z=4$, which is an ordered form of the β-Mn structure. The unit cell dimension was determined by x-ray powder diffraction to $a=6.4973(3)$ Å. In addition to the crystal structure, we have determined the magnetic structure and properties using superconducting quantum interference device magnetometry and Rietveld refinements of neutron powder diffraction data. A complex noncollinear magnetic structure is found, with magnetic moments of $2.97(4)\mu_B$ at 10 K only on the Mn atoms. The crystal structure consists of a triangular network built up by Mn atoms, on which the moments are rotated 120° around the triangle axes. The magnetic unit cell is the same as the crystallographic and carries no net magnetic moment. The Néel temperature was determined to be 210 K. A first-principles study, based on density functional theory in a general noncollinear formulation, reproduces the experimental results with good agreement. The observed magnetic structure is argued to be the result of frustration of antiferromagnetic couplings by the triangular geometry.

DOI: 10.1103/PhysRevB.69.054422 PACS number(s): 75.25.+z, 61.66.−f, 71.20.−b, 75.30.Cr

I. INTRODUCTION

The magnetic properties of different allotropes of elemental Mn and Mn-based compounds and alloys are conspicuous when compared to other transition-metal-based systems. With a few exceptions among the transition metals, it is for compounds containing Mn that one encounters noncollinear magnetism[1]—e.g., as witnessed in the α phase of Mn,[1] fcc Mn,[1] Mn_3Sn,[1] and Pd_3Mn.[2] Attempts have been made to understand why this is the case and first-principles calculations, based on a noncollinear formulation of density functional theory,[1,3,4] reproduce the magnetic properties of, e.g., Pd_3Mn,[5] fcc Mn,[1] Mn_3Sn,[1] and α-Mn.[6] One view for why Mn dominates in the class of noncollinear magnets is that for the early part of the transition metal series the interatomic exchange interactions are antiferromagnetic whereas for the later part the exchange is ferromagnetic.[7] Mn, being right in the middle of the series, hence has been suggested to balance these interactions by developing an exchange that is intermediate between ferromagnetism and antiferromagnetism—i.e., a noncollinear magnetic structure.[8] This view has to some extent been challenged lately,[9] with the argument that noncollinear magnetism is observed also for Fe (Ref. 1) and even Co-based (Ref. 10) compounds and alloys.

One of the allotropes of Mn, the β phase, reflects a very complex magnetic situation. Structurally the phase is stable between 725 °C and 1095 °C,[11] but it can be preserved at low temperatures by quenching. The primitive cubic crystal structure consists of two crystallographically inequivalent sites: one 8-fold and one 12-fold position.[12] For β-Mn several studies by both neutron diffraction,[13] polarized neutron scattering,[14] and NMR measurements[14] have not found any evidence of magnetic long-range order down to 4.2 K. However, solid solutions with other elements—e.g., Al—give rise to antiferromagnetic couplings for the Mn atoms situated on the 12-fold positions, whereas the Mn atoms on the 8-fold positions carry no magnetism.[14] There have been attempts to explain the lack of magnetic ordering by frustration of manganese spin moments on a three-dimensional triangular network built up by Mn atoms in 12-fold positions, which is suggested to result in a spin liquid that becomes spin glass like when other atoms are introduced.[14] The Mn magnetic moments in β-$(Mn_{1-x}Al_x)$ range from $1\mu_B$ to $1.5\mu_B$ in size[14] on the 12-fold site. This is in disagreement with a first-principles study that reports a moment of $0.2\mu_B$ only on Mn atoms located on the type-I site.[6] The type-I site would by common nomenclature correspond to the 8-fold position: however, this was not specified by the authors. Theoretical calculations for β-Mn have also been performed by, for instance, Sliwko *et al.* who within a theoretical model restricted to collinear couplings found a paramagnetic ground state, suggested to be close to ferrimagnetic order.[15]

Given the complexity of the magnetism of Mn-based compounds and, in particular, the β phase of Mn, it is of interest to examine the magnetic properties of other phases containing Mn, something we do here for the Ir-Mn-Si system for a phase with a crystal structure closely related to that of β-Mn. The ternary Ir-Mn-Si phase diagram has previously not been established: in fact, to our knowledge the only previous report in the literature of an ordered ternary compound of iridium, manganese, and silicon is a preliminary investigation of Mn_3IrSi by the present authors.[16] In the current article we report the crystal and magnetic structures of the new phase Mn_3IrSi and also present magnetization measurements and theoretical electronic structure and total energy calculations.

II. EXPERIMENT

A. Sample preparation

A sample of composition Mn_3IrSi was prepared by drop synthesis[17] in a high-frequency induction furnace. Single-

crystal pieces of silicon (Highways International, purity 99.999%) and pressed pellets of iridium powder (Alfa Aesar, purity 99.95%) were melted in an Al_2O_3 crucible under 300 mbar argon pressure. Pieces of manganese (Cerac, claimed purity 99.99%, purified from manganese oxides by sublimation) were dropped into the melt. After solidification the ingot was crushed and pressed into pellets, which were annealed in evacuated fused silica tubes at 900 °C for 3 days and at 800 °C for 1 week and subsequently quenched. After fine grinding the sample was stress relieved at 800 °C for 30 minutes.

B. X-ray powder diffraction

X-ray powder diffraction photographs were recorded at room temperature using a Guinier-Hägg focusing camera with Cu $K\alpha_1$ radiation and with silicon powder [$a = 5.43088(4)$ Å at 295 K] added as the internal standard for calibration. All diffraction lines could be indexed with a primitive cubic unit cell. The cell parameter was refined to $a = 6.4973(3)$ Å.

C. Neutron powder diffraction

Neutron powder diffraction data were collected at the Swedish research reactor R2 in Studsvik. Measurements were performed at 295 K, 80 K, and 10 K with the sample contained in a vanadium tube. The neutron beam was monochromated to 1.471 Å by two Cu(220) single crystals in parallel alignment. The diffractograms were recorded in the 2θ range $4° - 139.92°$ in steps of 0.08°. An absorption correction was applied using $\mu R = 0.715$, as calculated from a transmission measurement at $2\theta = 0°$.

D. Structure refinements

Structure refinements were performed according to the Rietveld method using the program FULLPROF (Ref. 18) with the scattering lengths Ir: 10.6 fm; Mn: −3.73 fm; Si: 4.149 fm. The background was modeled by interpolation between fixed points. A pseudo-Voigt profile function with a refined ratio of Gaussian and Lorentzian contributions was used to describe the peak shape. For iridium and silicon a common temperature factor was used due to severe correlation between the sites.

In the refinements performed for neutron powder diffraction data obtained at 295 K a total of 16 parameters were refined. Profile parameters: scale factor (1), zero point (1), profile shape parameter (1), half-width parameters (3), asymmetry parameters (2); structural parameters: atomic coordinates (5), unit cell dimension (1), isotropic temperature factors (2).

For the 10 K and 80 K data sets 18 parameters were refined: the x, y, and z-components of a magnetic moment placed on the manganese atoms, as well as the profile and structural parameters listed above, with the exception that an overall isotropic temperature factor was used. The magnetic form factor coefficients of Mn(0) were used. The nuclear and magnetic contributions to the diffraction intensities were treated as separate phases, with the magnetic phase modeled in space group $P1$. The starting model for the magnetic structure was obtained by reverse Monte Carlo simulations using the program RMCPOW.[19]

E. Magnetization measurements

The susceptibility was measured with a superconducting quantum interference device (SQUID) magnetometer in the temperature range from 50 K to 300 K with an applied field of 1000 G. Furthermore, the magnetization was measured as a function of applied field for $T = 50$ K and $T = 300$ K. The field was varied from −1500 G to 1500 G in steps of 100 G.

III. THEORY

The electronic structure and total energy calculations for Mn_3IrSi were based on density functional theory[20] (DFT) in the local density approximation.[21] We employed a scalar relativistic tight-binding linear-muffin-tin orbital method in the atomic sphere approximation[22,23] (TB-LMTO-ASA), including noncollinear spins[24] and the combined corrections in the one-electron Hamiltonian. The noncollinear magnetic structure can be described by assigning Cartesian coordinates for each atomic spin:

$$M_i = M(\sin\theta_i \cos\phi_i, \sin\theta_i \sin\phi_i, \cos\theta_i) = (M_{xi}, M_{yi}, M_{zi}),$$

where θ_i and ϕ_i are the polar angles of atom i and M the length of the magnetic moment M_i, having the x, y, and z components M_{xi}, M_{yi}, and M_{zi}. We relaxed the magnetic structure to the ground-state configuration by mixing of the polar angles. It should be noted that no symmetry constraints were imposed on the magnetic structure in the calculations. The calculations are converged with respect to the number of k points in the Brillouin zone, the size of the basis set (we used s, p, and d orbitals as basis functions for all atoms in the unit cell), and the self-consistency criterion. The Brillouin zone integration used a Gaussian broadening technique[25] where each eigenvalue is smeared with a width of 0.17 eV in order to speed up convergence.

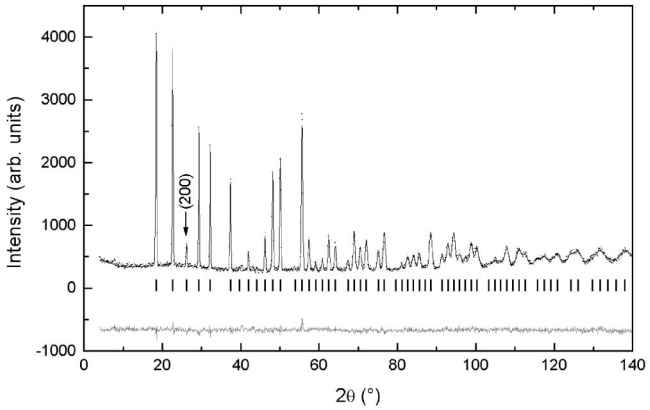

FIG. 1. Observed (dotted line), calculated (solid line), and difference (bottom line) neutron diffraction profiles at 295 K. Tick marks indicate the positions of Bragg reflections. The (200) reflection, allowed in space group $P2_13$, is indicated.

TABLE I. Refined structural parameters at 295 K. Estimated standard deviations in parentheses. Space group $P2_13$ (no. 198), unit cell parameter $a=6.4972(3)$ Å.

Atom	Wyckoff position	x	y	z	B_{iso} (Å^2)
Mn	12*b*	0.1181(9)	0.2074(9)	0.4546(8)	0.49(5)
Ir	4*a*	0.6833(3)	0.6833(3)	0.6833(3)	0.46(2)
Si	4*a*	0.0654(9)	0.0654(9)	0.0654(9)	0.46[a]

$R_p=4.29\%$, $R_{wp}=5.46\%$, $R_{expt}=4.64\%$, $\chi^2=1.39$, $R_{Bragg}=5.71\%$

[a]The isotropic temperature factors of Ir and Si were restrained to have the same value.

IV. RESULTS

A. Crystal structure

The crystal structure of Mn_3IrSi was found to be of the $AlAu_4$ type,[26] space group $P2_13$, with manganese in a 12*b* site and iridium and silicon in two separate 4*a* sites, which corresponds to four formula units per unit cell. In this structure type, which is an ordered form of the β-manganese structure type,[12] space group $P4_132$, the 8*c* site of β-Mn is split into two sets of fourfold positions which are occupied by different elements, while the 12-fold site is retained. For Mn_3IrSi, the ordering of Ir and Si on two different fourfold sites is evidenced by an observable (200) reflection (see Fig. 1), which is symmetry forbidden in space group $P4_132$ but allowed in $P2_13$. Examples of ternary compounds with the $AlAu_4$-type structure are $Mn_{33}Ni_{10}Si_7$ (Ref. 27) and $Cr_3Ni_5Si_2$, (Ref. 28); both phases are reported to have some mixed occupancy of the sites.

The structural parameters of Mn_3IrSi, as refined from neutron powder diffraction data at 295 K, are listed in Table I. Within experimental errors all three atomic sites are fully occupied, with no evidence of mixed occupancy. The agreement factors after the refinements were $R_{profile}=4.29\%$, $R_{wp}=5.46\%$, $R_{expt}=4.64\%$, $\chi^2=1.39$, and $R_{Bragg}=5.71\%$ for the 295 K data set. Interatomic distances shorter than 3.5 Å were calculated and are listed in Table II.

Manganese is effectively 14 coordinated in an irregular polyhedron, as illustrated in Fig. 2(a). In the polyhedron the three shortest Mn-Mn distances have been marked with dashed bonds. As illustrated in Fig. 2(b) these Mn atoms form a set of three equilateral triangles that are linked by the central Mn atom, with slightly different side lengths for the different triangles. All manganese atoms have the same surrounding, since there is only one crystallographic site for Mn. Thus a three-dimensional network of corner-linked Mn triangles stretches through the crystal structure, with each Mn atom shared between three triangles, as illustrated in the unit cell of Mn_3IrSi in Fig. 3. Both the iridium and silicon atoms are 12 coordinated by 9 Mn atoms and 3 Si or 3 Ir atoms, respectively, in a somewhat distorted icosahedral arrangement.

TABLE II. Interatomic distances at 295 K. Estimated standard deviations in parentheses.

Atoms	Distance (Å)	Atoms	Distance (Å)
Mn–Si	2.62(1)	Ir–3 Si	2.422(2)
Ir	2.688(6)	3 Mn	2.688(6)
2 Mn	2.691(9)	3 Mn	2.725(6)
Si	2.714(9)	3 Mn	2.729(5)
2 Mn	2.72(1)		
Ir	2.725(6)	Si–3 Ir	2.422(2)
Ir	2.729(5)	3 Mn	2.62(1)
2 Mn	2.774(9)	3 Mn	2.714(9)
Si	2.809(6)	3 Mn	2.809(6)
2 Mn	3.348(3)		

B. Magnetization measurements

The magnetization versus applied magnetic field, measured at 50 and 300 K, is shown in Fig. 4. The curves are closely linear and have almost the same slope. However, there is a weak nonlinearity and hysteresis that indicates the existence of a minor amount of ferromagnetic impurity in the sample (not resolved in the diffractograms). Disregarding this marginal artifact, we plot the measured susceptibility (M/H) versus temperature in an applied field of 1 kG in Fig. 5(a). The temperature dependence of the susceptibility shows a weak maximum at about 225 K, indicating an antiferromagnetic state at low temperatures. From the maximum in the $d(\chi T)/dT$ versus temperature curve, shown in Fig. 5(b), the antiferromagnetic transition is found to occur at about 210 K [employing the relation $d(\chi T)/dT \propto C_m$, where C_m is the magnetic specific heat, derived by Fisher[29]]. The susceptibility is quite weakly temperature dependent and decays

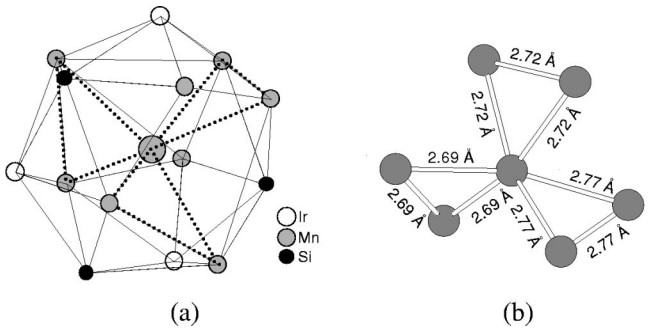

FIG. 2. Coordination geometry around manganese. (a) 14 CN polyhedron (central Mn atom enlarged). (b) The triangles of Mn atoms, building up the triangular network (distances at 295 K displayed).

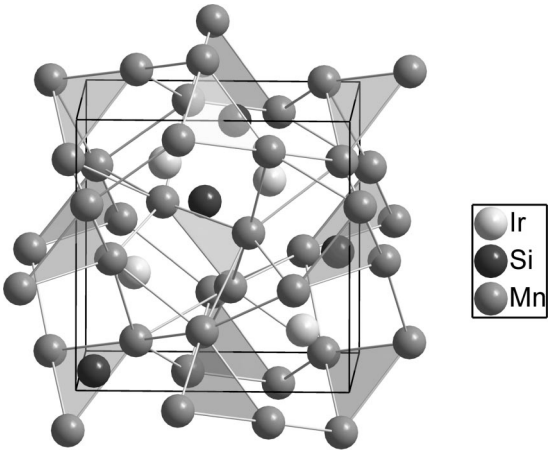

FIG. 3. The crystal structure of Mn_3IrSi. The triangular network and the unit cell are indicated and one type of Mn triangle is shaded.

only very slowly at temperatures above the maximum. If we assume a Curie-Weiss behavior at temperatures above the antiferromagnetic transition temperature (T_N), the slow decay indicates that the Weiss temperature (θ_W) is very large compared to T_N. Such a difference is characteristic of highly frustrated magnetic systems.[30] Unfortunately, our measurement system does not allow high-temperature measurements, so we have no possibility to explore temperatures high enough to extract an experimental θ_W value.

C. Experimental magnetic structure

The neutron powder diffractograms recorded at 10 K and 80 K both have magnetic contributions to the observed intensities; two peaks not present at room temperature emerge (indexed in Fig. 6) and some peaks display higher intensities at low temperatures. The magnetic contribution to the diffraction pattern is shown separately in the inset to Fig. 6, where the calculated nuclear contribution has been subtracted from the observed total intensity. It should however

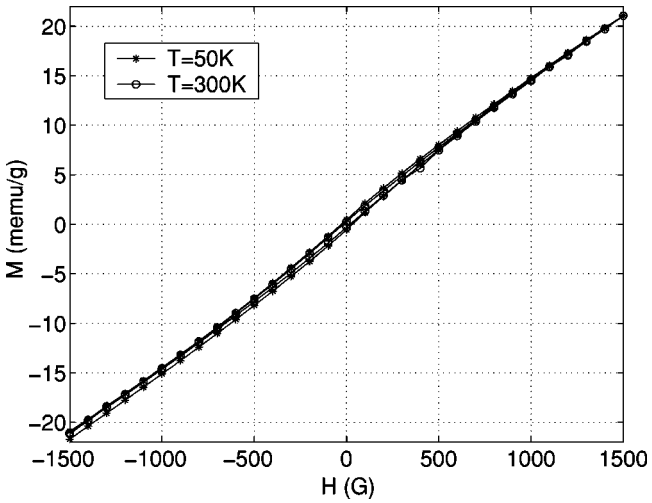

FIG. 4. The magnetization as a function of the applied field for $T=50$ K and 300 K.

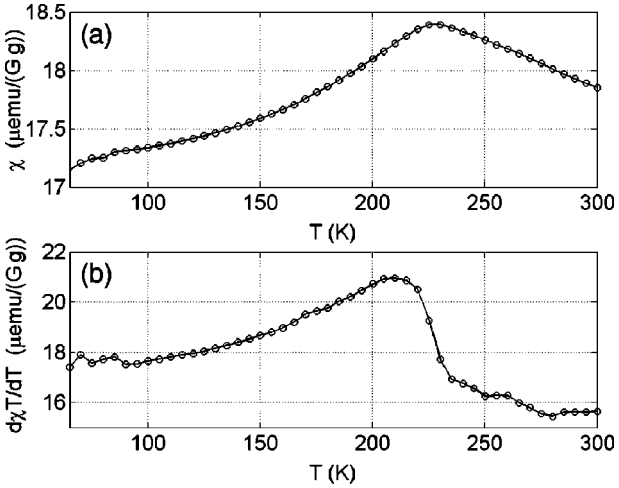

FIG. 5. (a) The temperature dependence of the magnetic susceptibility (χ) measured with an applied field of 1 kG. (b) $d(\chi T)/dT$ vs temperature. Note that the vertical axes have been truncated.

be noted that this plot also contains the differences between the observed and calculated nuclear diffraction intensities, which give rise to the somewhat noisy base line. All magnetic contributions can be explained by a magnetic unit cell of the same size as the crystallographic, but of lower symmetry, with magnetic moments only on the manganese atoms. The refined structural parameters and total magnetic moment at 10 K can be found in Table III. The agreement factors were $R_{profile}=4.59\%$, $R_{wp}=5.85\%$, $R_{expt}=4.75\%$, $\chi^2=1.52$, $R_{Bragg}=5.44\%$, and $R_{mag}=7.94\%$. No significant difference from the values obtained for the 10 K data set was noted in refinements of the 80 K data.

For the Mn atom with position coordinate (0.1195, 0.2031, 0.4573) the total magnetic moment $M=2.97(4)\mu_B$ at 10 K has the vector components $M_x=1.3(1)\mu_B$, $M_y=2.3(1)\mu_B$, and $M_z=-1.4(1)\mu_B$. The directions of the

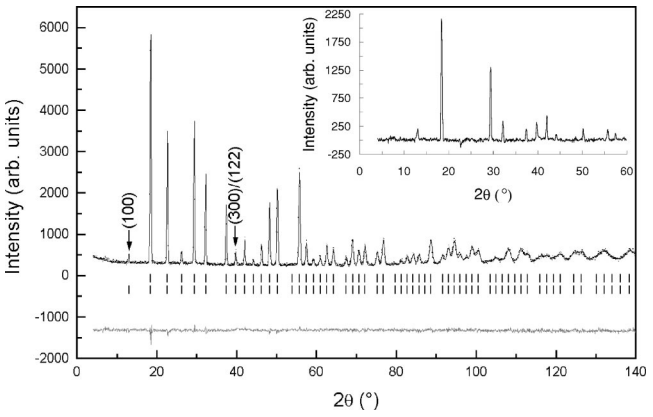

FIG. 6. Observed (dotted line), calculated (solid line), and difference (bottom line) neutron diffraction profiles at 10 K. Upper tick marks indicate the positions of Bragg reflections for the crystal structure, lower tick marks for the magnetic structure. Pure ''magnetic'' reflections, symmetry forbidden for the crystal structure, are indicated. The inset shows only the magnetic intensity, obtained by subtracting the calculated nuclear contribution from the observed total intensity.

TABLE III. Refined structural parameters and magnetic moment at 10 K. Estimated standard deviations in parentheses. Unit cell parameter $a=6.4879(2)$ Å.

Atom	Wyckoff position	x	y	z	M (μ_B)
Mn	12*b*	0.1195(8)	0.2031(9)	0.4573(8)	2.97(4)
Ir	4*a*	0.6825(3)	0.6825(3)	0.6825(3)	
Si	4*a*	0.0635(9)	0.0635(9)	0.0635(9)	

$B_{\text{overall}}=0.16(2)$ Å^2

$R_p=4.59\%$, $R_{\text{wp}}=5.85\%$, $R_{\text{expt}}=4.75\%$, $\chi^2=1.52$, $R_{\text{Bragg}}=5.44\%$, $R_{\text{mag}}=7.94\%$

magnetic moments on all 12 Mn atoms in the unit cell can be generated from this vector by symmetry operations of the crystallographic space group. For the atoms with coordinates generated by a 2_1 screw operation, the components of the magnetic moments that are perpendicular to the 2_1 axis are rotated 180° around the axis. Thus the (100) and (300) reflections that are symmetry forbidden for the crystal structure show observable magnetic diffraction intensities, as can be seen in Fig. 6.

In the crystal structure nonintersecting threefold rotation axes parallel to the different ⟨111⟩ directions of the cubic unit cell pass through the centers of the manganese triangles that were previously described in Fig. 2(b). These threefold rotation axes are preserved in the magnetic structure. For three Mn atoms on a triangle this threefold rotation results in a 120° rotation of the projection of the magnetic moment vector on the triangle plane. However, the three magnetic moment vectors all have small angles out of the triangle planes, resulting in small net magnetic moments of the triangle units, the net moments being parallel to a ⟨111⟩ direction. The orientations of the moments on three corner sharing triangles are illustrated in Fig. 7(a).

One way of building up the crystal structure is by repeating only the triangle that is smallest at 10 K (2.68 Å, shaded in Fig. 3). The two other triangles in the network are then formed by linking together the small triangles. For the 2.68 Å triangle unit the moments point outwards from the center, as illustrated in Fig. 7(b). The net moment of this triangle unit, resulting from the small out-of-plane components of the magnetic moments, is canceled when the moments on all 12 Mn atoms in the unit cell are generated by the symmetry operations described above. The four equivalent 2.68 Å triangles thus generated, with the net moments placed in the centers, are illustrated in Fig. 8.

D. Theoretical magnetic structure

Several magnetic configurations for the Mn atoms in Mn_3IrSi have been investigated: ferromagnetic, collinear antiferromagnetic, and the experimental noncollinear antiferromagnetic arrangement described earlier in this paper. First-principles total energy calculations of the mentioned magnetic structures were performed in order to find the ground state of Mn_3IrSi. The calculations were achieved using the lattice parameters determined experimentally at room temperature, which are displayed in Table I. The ferromagnetic arrangement of the Mn atoms turned out to be the highest in energy. Four different kinds of collinear antiferromagnetic arrangements of the Mn atoms were considered in our investigation. All of them had lower energy than the ferromagnetic configuration. The noncollinear antiferromagnetic orientation of the spins, as suggested by experiments, is the configuration that has the lowest energy among all the studied magnetic orderings. Taking the energy of the experimental noncollinear state as a reference, we found that the ferromagnetic configuration is 17 mRy higher in energy and that the four different collinear antiferromagnetic orientations considered here are approximately 6–7 mRy above the experimental configuration, but below the ferromagnetic energy. In Fig. 9 we have schematically presented the energies

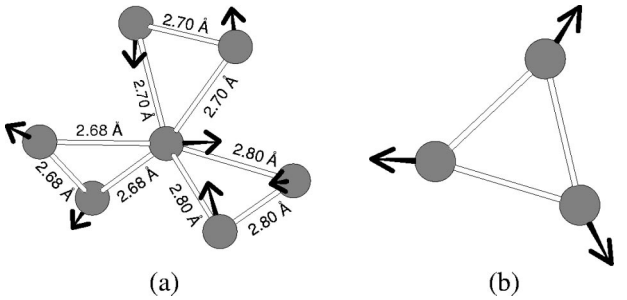

FIG. 7. (a) Orientation of the magnetic moments on the three linked Mn triangles. Mn-Mn distances at 10 K displayed, with the magnetic moments illustrated as vectors of arbitrary length. (b) Triangular unit of 2.68 Å Mn-Mn distances.

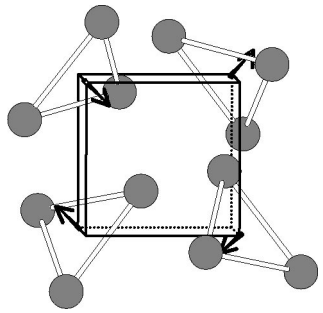

FIG. 8. Net magnetic moments of the 2.68 Å Mn triangles illustrated as arrows pointing along four different ⟨111⟩ directions and thus canceling one another. The illustration box corresponds to one-half of the unit cell edges.

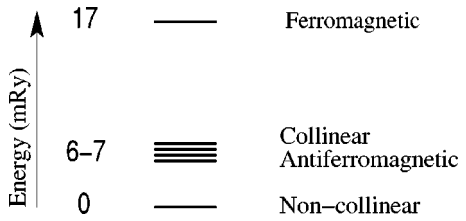

FIG. 9. Schematic representation of the calculated total energies of the magnetic structures considered in the present investigation. The most energetically stable configuration is the noncollinear structure proposed by experiments.

of the configurations considered in the present study. It is interesting to note that the four collinear antiferromagnetic orderings have similar energies, which is consistent with frustrated antiferromagnetic interactions. It is well known that in some crystal structures it is not possible to satisfy all exchange interactions if they are antiferromagnetic and of nearest-neighbor nature—for instance, in the two-dimensional triangular network or the fcc lattice. In that case the system possesses a multiplicity of equally unsatisfied states and is said to show frustration.[1] A way to lower the energy is then to form a noncollinear magnetic structure and we propose that this is the situation in Mn_3IrSi.

We proceeded the theoretical analysis by self-consistent calculations, where not only the charge and spin densities were allowed to be updated from iteration to iteration, but also the polar angles determining the direction of the magnetic moments were calculated self-consistently.[3] In Table IV we compare the so calculated x, y, and z components of the magnetic moments to the experimental values for every manganese atom in the unit cell. The agreement between the experimental values and those calculated theoretically is remarkable, especially considering the complexity of the experimental magnetic structure. The manganese atoms ordered in this noncollinear manner have a calculated magnetic moment of $\sim 3.0\mu_B$ and the Ir and Si atoms have small moments of $0.03\mu_B$ and $0.01\mu_B$, respectively. Hence we conclude that not only the directions of the magnetic moments, but also the magnitudes are well reproduced by theory. It should be noted that for ferromagnetic compounds and alloys, a similar, excellent agreement between experiment and theory is normally found.[1,3,31] Although less experience has been gained for noncollinear systems, the data that are available[1,3] suggest that DFT-based methods reproduce the magnetic moments of these systems with great accuracy.

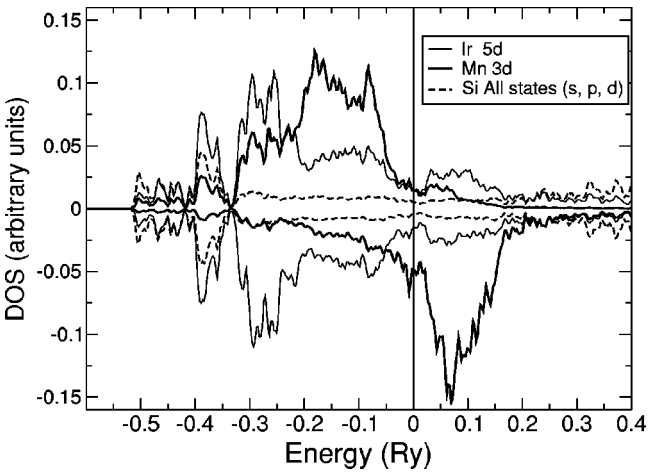

FIG. 10. The calculated density of states of Mn_3IrSi. The energies are given relative to the Fermi energy, which is indicated by a vertical line.

In order to present a complete picture of the new phase Mn_3IrSi, we show in Fig. 10 the density of states (DOS) of Mn_3IrSi. Note that negative densities represent the spin-down states. All Si states (s, p, and d) are summed and depicted in Fig. 10 (dashed line): we also show the Ir $5d$ states, which correspond to the thinner solid line. The thickest solid line represents the Mn $3d$ states. From the figure it is possible to see that the spin splitting is approximately 0.3 Ry for Mn and that no significant exchange splitting is found

TABLE IV. Comparison between calculated and experimental values of the x, y, and z components (M_x, M_y, M_z) of the magnetic moment. The Mn atoms are numbered as the equivalent coordinates of the 12b site in space group $P2_13$ in the International Tables for Crystallography.

	Calculated			Experimental		
Atom	M_x	M_y	M_z	M_x	M_y	M_z
Mn 1	1.05	2.37	−1.52	1.3(1)	2.3(1)	−1.4(1)
Mn 2	−1.09	−2.37	−1.49	−1.3(1)	−2.3(1)	−1.4(1)
Mn 3	−1.12	2.34	1.51	−1.3(1)	2.3(1)	1.4(1)
Mn 4	1.05	−2.37	1.52	1.3(1)	−2.3(1)	1.4(1)
Mn 5	−1.58	1.30	2.19	−1.4(1)	1.3(1)	2.3(1)
Mn 6	−1.63	−1.29	−2.16	−1.4(1)	−1.3(1)	−2.3(1)
Mn 7	1.58	−1.30	2.20	1.4(1)	−1.3(1)	2.3(1)
Mn 8	1.58	1.30	−2.19	1.4(1)	1.3(1)	−2.3(1)
Mn 9	2.30	−1.32	1.40	2.3(1)	−1.4(1)	1.3(1)
Mn 10	−2.28	−1.33	−1.42	−2.3(1)	−1.4(1)	−1.3(1)
Mn 11	2.30	1.31	−1.42	2.3(1)	1.4(1)	−1.3(1)
Mn 12	−2.30	1.34	1.38	−2.3(1)	1.4(1)	1.3(1)

for Si and Ir. The large spin splitting in Mn is consistent with the large magnetic moments found on those atoms. It is also interesting to note that there is some hybridization between the Ir and Mn states, whereas the Si states are distributed over a large energy interval.

V. CONCLUSIONS

A new phase, Mn_3IrSi, has been synthesized and found to crystallize in the $AlAu_4$-type structure, an ordered form of the β-Mn structure. In contrast to pure β-Mn, Mn_3IrSi is magnetically ordered below the Néel temperature (210 K). Localized magnetic moments in the β-Mn structure have previously been observed—e.g., on Al substitution $(Mn_{1-x}Al_x)$.[14] The magnetic structure of Mn_3IrSi is complex with noncollinear moments of approximately $3\mu_B$ only on the Mn atoms. The Mn atoms form a triangular network on which the moments are rotated 120° around the triangle axes. The magnetic unit cell is of the same size as the crystallographic and has no net magnetic moment. Our first-principles calculations reproduce with good agreement the experimental magnitude and orientation of the atomic magnetic moment. The microscopic origin of the exchange interactions has been found to be antiferromagnetic couplings between Mn atoms. The observed magnetic structure is argued to be the result of the frustration of these antiferromagnetic interactions by triangular geometry. Comparing the magnitude of the interaction energies involved in the ordering of Mn_3IrSi (20 mRy) with the corresponding energies and transition temperatures for some unfrustrated systems (Fe, Co, and Ni),[1,3] we find that the ordering temperature of Mn_3IrSi would have been of the order of 700–1000 K in an unfrustrated geometry. The much lower value of the measured transition temperature (210 K) confirms that geometric frustration is of crucial importance for magnetic ordering in Mn_3IrSi.

ACKNOWLEDGMENTS

Håkan Rundlöf is acknowledged for skillful assistance in neutron powder diffraction data collection. We are grateful to Dr. Anders Mellergård for aid in setting up simulations by the program RMCPOW. Financial support from the Swedish Research Council (VR) and the Swedish Foundation for Strategic Research (SSF) is acknowledged. O.E. is grateful to the Göran Gustafsson Foundation for support.

[1] J. Kübler, *Theory of Itinerant Electron Magnetism* (Oxford Science Publications, Oxford, 2000).
[2] P. Önnerud, Y. Andersson, R. Tellgren, and P. Nordblad, J. Solid State Chem. **128**, 109 (1997).
[3] L. M. Sandratskii, Adv. Phys. **47**, 91 (1998).
[4] L. Nordström and D. J. Singh, Phys. Rev. Lett. **76**, 4420 (1996).
[5] P. H. Andersson, L. Nordström, and O. Eriksson, Phys. Rev. B **60**, 6765 (1999).
[6] D. Hobbs and J. Hafner, J. Phys.: Condens. Matter **13**, L681 (2001).
[7] V. Heine and J. H. Samson, J. Phys. F **13**, 2155 (1983).
[8] S. Blugel, B. Drittler, R. Zeller, and P. H. Dederichs, Appl. Phys. A: Solids Surf. **49**, 547 (1989).
[9] R. Lizárraga *et al.* (unpublished).
[10] R. Berger, M. Fritzsche, A. Broddefalk, P. Nordblad, and B. Malaman, J. Alloys Compd. **343**, 186 (2002).
[11] W. B. Pearson, *A Handbook of Lattice Spacings and Structures of Metals and Alloys* (Pergamon Press, Belfast, 1958).
[12] G. D. Preston, Philos. Mag. **5**, 1207 (1928).
[13] J. S. Kasper and B. W. Roberts, Phys. Rev. **101**, 537 (1956).
[14] H. Nakamura, K. Yoshimoto, M. Shiga, M. Nishi, and K. Kakurai, J. Phys.: Condens. Matter **9**, 4701 (1997).
[15] V. Sliwko, P. Mohn, and K. Schwarz, J. Phys.: Condens. Matter **6**, 6557 (1994).
[16] T. Eriksson, S. Felton, R. Lizárraga, O. Eriksson, P. Nordblad, and Y. Andersson, J. Magn. Magn. Mater., proceedings ICM-03 (to be published).
[17] S. Rundqvist, Chem. Scr. **28**, 15 (1988).
[18] J. Rodríguez-Carvajal, computer program FULLPROF, version 2.10, LLB, Saclay, 2002.
[19] A. Mellergård and R. L. McGreevy, Mater. Sci. Forum **378–381**, 71 (2001).
[20] P. Hohenberg and W. Kohn, Phys. Rev. **136**, B864 (1964).
[21] U. von Barth and L. Hedin, J. Phys. C **5**, 1629 (1972).
[22] O. K. Andersen, Phys. Rev. B **12**, 3060 (1975).
[23] H. L. Skriver, *The LMTO Method* (Springer, Berlin, 1984).
[24] The computer code was made in-house, based on the original method published in Ref. 22. For details see www.fysik.uu.se/theomag
[25] M. Methfessel and A. T. Paxton, Phys. Rev. B **40**, 3616 (1989).
[26] O. E. Ullner, Ark. Kemi, Mineral. Geol. **14A**, 1 (1940).
[27] C. B. Shoemaker, D. P. Shoemaker, T. E. Hopkins, and S. Yindepit, Acta Crystallogr., Sect. B: Struct. Crystallogr. Cryst. Chem. **34**, 3573 (1978).
[28] E. I. Gladyshevskii, P. I. Kripyakevich, and Y. B. Kuz'ma, Zh. Strukt. Khim. **3**, 414 (1962) [J. Struct. Chem. **3**, 402 (1962)].
[29] M. E. Fisher, Philos. Mag. **7**, 1731 (1962).
[30] A. S. Wills, Can. J. Phys. **79**, 1501 (2001).
[31] P. James, O. Eriksson, B. Johansson, and I. A. Abrikosov, Phys. Rev. B **59**, 419 (1999).